

Probing The Cosmological Constant Through The Alcock-Paczynski Test Based on The Lyman-Alpha Forest

Wen-Ching Lin^{1,2,3} and Michael L. Norman^{1,2}

ABSTRACT

In recent years, the possibility of measuring the cosmological constant Ω_Λ through the application of the Alcock-Paczynski test to the Lyman Alpha ($\text{Ly}\alpha$) forest has been suggested (McDonald et al. 1999; Hui et al. 1999). Some of the greatest difficulties we encounter concern the huge uncertainty of observational data due to cosmic variance and noise. In this paper, we propose a maximum likelihood estimation (MLE) method to deal with cosmic variance using synthetic spectra of quasistellar objects (QSOs) from our cosmological hydrodynamic simulations with noise added. We have demonstrated that the MLE method can overcome the cosmic variance problem. Applying the MLE method, we find that we have more than 90 % probability to determine Ω_Λ within 20 % error and approximately of 66% probability to determine Ω_Λ within 10 % error by using 30 pairs QSO spectra. Another important source of error is from noise in the flux spectra, and we have modeled the corresponding effect by studying artificial spectra with different kinds of noise added. We discover that the noise distribution does not have significant effect on the final cross-correlation functions as long as the signal-to-noise ratio (S/N) is fixed. We also find that with $S/N = 10$, the corresponding uncertainty in Ω_Λ is much larger than the uncertainty caused by cosmic variance. With $S/N = 20$ the uncertainty in Ω_Λ is reduced and is compatible in magnitude to the error due to cosmic variance. Therefore, we conclude that spectra with $S/N \geq 20$ are desirable to achieve an useful result.

Subject headings: Ly α forest, cosmological constant, AP test

¹Physics Department, University of California at San Diego, San Diego, CA 92093

²Center for Astrophysics and Space Sciences, University of California at San Diego, San Diego, CA 92093

³Astronomy Department, University of Illinois, Urbana, IL 61801

1. Introduction

An important topic in cosmology is the determination of the energy densities of the various components of the Universe. Therefore constraining the values of their respective fractional energy densities: baryon density (Ω_B), matter density (Ω_M) and vacuum density (Ω_Λ) becomes a vital part of understanding the Universe. Current Boomerage data indicates $0.85 \leq \Omega_0 \leq 1.25$ (Melchiorri et al. 2000) and more data is on the way (Python V, Viper, Mat, Maxima, Boomerang, DASI, NASA's MAP, ESA's PLANCK). As for Ω_B , the Burles-Tytler measurement gives $\Omega_B h^2 = 0.019 \pm 0.0012$ (Tytler 1999; Burles et al. 1999), which is consistent with several other results (Meiksin & Madau 1993; Copi et al. 1995, Hata et al. 1995; Rauch et al. 1997; Weinberg et al. 1997). On the other hand, the total matter density Ω_M can be inferred from the BBN baryon density and rich clusters data (White et al. 1993). The value of Ω_M is believed to be 0.4 ± 0.1 based on estimates using various physical phenomenon (Mohr et al. 1998; Carlstrom et al. 1999; Bahcall & Fan 1998; Bahcall 2000; Peacock & Dodds 1994).

The results $\Omega_0 = 1 \pm 0.2$ and $\Omega_M = 0.4 \pm 0.1$ suggest the existence of a dark, exotic form of energy, which is smoothly distributed and contributes roughly 60% of the critical density (Turner et al, 1983; Peebles, 1984). It is summarized $\Omega_\Lambda = \frac{4}{3} \Omega_M + \frac{1}{3} \pm \frac{1}{6}$ based on observations of the Type Ia supernovae (Perlmutter et al. 1999; Goobar 2000; Riess et al. 1998; Schmidt et al. 1998), which is consistent with studies based on different physics (Holder et al. 2000; Guerra et al. 2000). Since all these results are based on data at $z < 2$ (mostly < 1), other independent measurements of Ω_Λ from data at an earlier epoch becomes important. This motivates us to implement the Alcock-Paczynski Test (AP test) on the Lyman Alpha ($\text{Ly}\alpha$) forest.

In 1979, Alcock and Paczynski proposed a method which can be used to measure the geometry of the Universe (Alcock & Paczynski, 1979). The basic idea of this method is that for a spherical object in the sky, its physical size along the line of sight and perpendicular to the line of sight should be equal. This method can be extended to non-spherical cosmological structures, in which case the characteristic length of the correlation function of the structure will be used instead of the physical size of the object. The two-point correlation functions of galaxies and clusters have been suggested as candidates for the AP test (Ryden 1995; Ballinger et al. 1996; Matsubara & Suto 1996; Popowski et al. 1998). Recently the cross-correlation function of $\text{Ly}\alpha$ forest clouds has been proposed as a good candidate for the AP test as well (McDonald et al. 1999; Hui et al. 1999).

The geometrical basis of the AP test suggests the measurement of the value $\frac{\Delta z}{z\Delta\theta}$, where $\frac{\Delta z}{z}$ and $\Delta\theta$ relate to the scales of the object due to the Hubble flow expansion parallel and perpendicular to the line of sight, respectively. Observationally, the characteristic lengths

parallel and perpendicular to the line of sight can be written in terms of the velocity separations v_{\parallel} and v_{\perp} . The velocity parallel to the line of sight is given by :

$$\Delta v_{\parallel} = \frac{\Delta z}{1+z}c = \Delta v_h + \Delta v_p \quad (1)$$

where Δv_h is the velocity separation due to the Hubble flow expansion and Δv_p denotes the effect of the peculiar velocity. The transverse velocity separation is :

$$\Delta v_{\perp} = H(z)\Delta l = H(z)D_A(z)\Delta\theta \quad (2)$$

where $D_A(z)$ is the redshift-dependent angular diameter distance, $H(z)$ is the expansion rate and Δl is the physical size of the object we are interested in. We can write Δv_{\perp} in a form expressing its relationship with cosmological parameters explicitly : $\Delta v_{\perp} = c f(z) \Delta\theta$, where

$$f(z) = \frac{1}{c}D_A(z)H(z) = \frac{E(z)}{1+z} \int_0^z \frac{dz'}{E(z')} \quad (3)$$

with $E(z) = [\Omega_m(1+z)^3 + \Omega_{\Lambda}(1+z)^{3(1+\omega)}]^{\frac{1}{2}}$ where we specialize to the case with an equation of state $\omega \equiv \frac{dp}{d\rho} = -1$.

Because the matter distribution expands with the Hubble flow at the same rate in all directions in a homogeneous and isotropic universe, the formation of structures should be equal in all directions statistically. Therefore, the auto-correlation function along the line of sight $\xi(\Delta v_{\parallel})$ and the auto-correlation function perpendicular to the line of sight $\xi(\Delta v_{\perp})$ should be the same. Unfortunately, it is impossible to determine the auto-correlation function perpendicular to the line of sight $\xi(\Delta v_{\perp})$ observationally. However, we can overcome this problem by observing the flux spectra of a pair of quasistellar objects (QSOs) and derive the corresponding cross-correlation function $\xi_{\times}(\Delta v_{\parallel}) = \xi_{\times}(\sqrt{\Delta v^2 - \Delta v_{\perp}^2})$. From Equation (2) and Equation (3), we know that Δv_{\perp} is very sensitive to cosmology as is the cross-correlation function $\xi_{\times}(\sqrt{\Delta v^2 - \Delta v_{\perp}^2})$ (McDonald et al. 1999).

Figure (1) shows the cross-correlation functions in different cosmological models as taken from our simulations. Here we use fully hydrodynamic simulations to provide realistic cross-correlation functions in different cosmological models instead of using semi-analytic calculations based on N-body simulations. Because our fully hydrodynamic code includes gas dynamics, the peculiar velocity effect has also been taken into account. In this specific structure, the Ly α forest, at redshift 2, the velocity separations of 100 - 600 km/s correspond to comoving scales of 1 - 10 Mpc, which is the characteristic size of voids. Most Ly α forest absorbers correspond to the low overdensity regions in the voids (Zhang et al. 1998),

so the gases therein expand with Hubble flow instead of collapsing gravitationally, which makes them perfect candidates for the AP test.

This paper is organized as follows : The cosmological simulations and the analysis codes are discussed in §2 and §3. Then we display our methodology in §4. Finally, we provide our results and concluding remarks in §5 and §6. The additional information about maximum likelihood estimation and error propagation are given in Appendix (A) and Appendix (B).

2. Cosmological Simulations

2.1. Cosmological Code

We have performed several simulations of the $z = 2$ Ly α forest in different cosmological models. All simulations were performed using our adaptive mesh refinement (AMR) cosmological hydrodynamics code Enzo. Enzo incorporates a Lagrangean particle-mesh (PM) algorithm to follow the collisionless dark matter and a higher-order accurate piecewise parabolic method (PPM) to solve the equations of gas dynamics. In addition to the usual ingredients of baryonic and dark matter, Enzo also solves a coupled system of non-equilibrium ionization equations with radiative cooling for a gas with primordial abundances. Our chemical reaction network includes six species: HI, HII, HeI, HeII, HeIII and e^- (Abel et al. 1997; Anninos et al. 1997). The simulation starts with the initial perturbations originating from inflation-inspired adiabatic fluctuations. The BBKS (Bardeen et al. 1986) transfer function is employed with the standard Harrison-Zel’dovich power spectrum. Another important component in the simulations is an ultraviolet (UV) radiation background which ionizes the neutral intergalactic medium. Haardt & Madau (1996) have provided a UV radiation field with radiation transfer in a clumpy universe based upon the observed quasar luminosity function. Enzo starts to import their homogeneous UV background spectra at redshift 7 and increases the intensity of the spectra at redshift 6 to generate photoionization and photoheating rates in our simulations.

2.2. Ly α Forest Simulations

In this work we performed six Ly α forest simulations using Enzo. All simulations were done on the Origin 2000 supercomputer at the National Center for Supercomputing Applications (NCSA). The comoving box sizes of our simulations are 37.3 Mpc (25.73 Mpc/h) with 256^3 dark matter particles and a 256^3 grid for the evolution of gas dynamics. The cosmological parameters used here are $\sigma_8 = 0.73$, $\Omega_B = 0.04$, $\Omega_{total} = 1.0$, $h = 0.69$ and the

power spectrum index $n = 1.0$. The only parameter varied over the 6 simulations is Ω_Λ , which is given values of 0.0, 0.5, 0.6, 0.7, 0.8 and 0.9.

3. Artificial QSO spectra

3.1. Spectrum Generator

In order to compare our simulation results to observations, we need to produce realistic artificial flux spectra from our simulations. The spectrum generator we used here starts at the point with the lowest neutral hydrogen density inside the box, shooting photons along random lines of sight through the box. It calculates the transmitted flux of a QSO at redshift z as $e^{-\tau_\nu}$, with the optical depth τ_ν given by

$$\tau_\nu(t) \equiv \int_t^{t_0} n_{HI}(t) \sigma_\nu c dt \quad (4)$$

where c is the speed of light, n_{HI} is the number density of the HI absorbers, σ_ν is the absorption cross-section, and t is the cosmic time. Integration is performed along the line of sight from the QSO to the observer. This can be written in a form more suitable for computation (Zhang et.al. 1997) as

$$\tau_\nu(z) = \frac{c^2 \sigma_o}{\sqrt{\pi} \nu_o} \int_z^{z_o} \frac{n_{HI}(\hat{z}) a^2}{b} \frac{d\hat{z}}{a} \exp \left\{ - \left[(1 + \hat{z}) \frac{\nu}{\nu_o} - 1 + \frac{v}{c} \right]^2 \frac{c^2}{b^2} \right\} d\hat{z}$$

where z is the redshift, σ_o is the resonant Ly- α cross section, ν_o is the Ly α rest frequency, $b = \sqrt{2kT/m_p}$ is a measure of the effect of Doppler broadening on the absorption cross section, v is the peculiar velocity along the line-of-sight and ν is the redshifted frequency. This equation, parametrized to order v/c , needs the scale factor a to be specified, which is given by the Friedman equation,

$$\dot{a} = H_o \sqrt{1 + \Omega_m \left(\frac{1}{a} - 1\right) + \Omega_\Lambda (a^2 - 1)}$$

The resolution and length of the spectra is a free parameter specified by the user.

In order to generate paired QSO spectra, we first calculated the comoving separation d of two QSOs at the desired redshift based on the known angular separation under a given cosmological model. Then from the point with the lower neutral hydrogen density, point A , and a given random direction \vec{r} , the plane $S : (\vec{x} - A) \cdot \vec{r} = 0$ is uniquely determined. Then on the circle with center A and radius $d/2$ on S , we chose two points C and D where C-A-D lay on a line. Then we generated two parallel QSO spectra from C and D both along the direction \vec{r} . Figure (2) shows a pair of simulated QSO spectra with a resolution identical to

the Low Resolution Imaging Spectrometer (LRIS) on the Keck telescope:

3.2. Spectra Degrading and Signal to Noise Properties

In order to compare with the observational data, we degrade our ideal spectra to the resolution of the desired instrument. The resolution of each ideal QSO spectrum was degraded by convolving the entire spectrum with a normalized Gaussian function :

$$f(x) = \frac{1}{\sigma\sqrt{2\pi}} \exp\left[-\frac{x^2}{2\sigma^2}\right] \quad (5)$$

with $\sigma = \frac{FWHM}{8\sqrt{\ln 2}}$, where FWHM is the full width half maximum of the spectral resolution of the desired instrument. The convolution subroutine used was based on FFT algorithms from Numerical Recipes (Press et al.,1988). Figure (3) shows the degraded simulated spectra at different resolutions.

We also examined the effect of different S/N in our simulated spectra based on Gaussian-distributed noise. The noise comes from a Gaussian distribution with zero mean and unit variance:

$$p(y)dy = \frac{1}{\sqrt{2\pi}} \exp[-y^2/2]dy \quad (6)$$

and we denote the noise as N_{gauss} . Then with a given S/N value, we derived the final flux spectra by adding the corresponding noise to the original flux spectra:

$$f_{final} = f_{orig} + \frac{N_{gauss}}{S/N} \quad (7)$$

where f_{final} is the final flux with noise and f_{orig} the flux after degrading the spectrum. Adding noise to spectra introduces small scale power. To study this, we first define the overflux δ_f as $\frac{f-f}{\bar{f}}$, where \bar{f} is the mean flux of the spectrum at a given redshift interval ($1.754 \leq z \leq 1.954$ in this paper) and is calculated by averaging the whole data points in the spectrum. So we have :

$\delta_f(z_1), \delta_f(z_2), \dots, \delta_f(z_n)$ from a QSO spectrum, where $z_i, i= 1,2 \dots, n$ are the corresponding redshifts at each data point.

Therefore, the flux power spectrum $P^f(k)$ is defined as :

$$P^f(k_i) = \sum_{j=0}^{n-1} \delta_f(z_j) \exp\left[-2\pi i j \frac{\sqrt{-1}}{n}\right] \quad (8)$$

and is calculated by the Fastest Fourier Transform of the West (Frigo et al. 1998). Figure (4) shows that when degrading a QSO spectrum, the amplitude of the flux power spectrum

decreases. On the other hand, adding noise also increases the amplitude of the flux power spectrum. Beyond $k = 0.1 \text{ rad}/(\text{km/s})$ (where rad denotes the unit of 2π) the noise dominates the amplitude of the power spectrum. This tells us that the data beyond $k = 0.1 \text{ rad}/(\text{km/s})$ is not reliable, due to the noise effect.

Because the distribution of noise in the observation is unknown, we chose several common distributions of noise added to our simulated spectra for the analysis work. We compared the results based on Gaussian-distributed noise with other noise distributions including the Poisson and Gamma distributions. We used the routines in Numerical Recipes (Press et al., 1988) to generate noise from the above distributions. For a Poisson distribution, the total probability of integer j (event j) is :

$$Prob(j) = \int_{j-\epsilon}^{j+\epsilon} P_x(m) dm = \frac{x^j e^{-x}}{j!} \quad (9)$$

The Poisson noise, $N_{poisson}$ is a random deviate drawn from the Poisson distribution with unit mean. Similarly, a Gamma distribution of integer order $a \geq 0$ is the waiting time to the a_{th} event in a Poisson random process of unit mean. We know that a Gamma deviate has a probability $P_a(x)dx$ of occurring with a value between x and $x + dx$, where

$$P_a(x)dx = \frac{x^{a-1} e^{-x}}{\Gamma(a)} dx, x \geq 0 \quad (10)$$

where $\Gamma(x)$ is the gamma function. Then the noise is a deviate distributed as a gamma distribution of integer order 1, which is the waiting time to the first event in a Poisson process of unit mean. Figure (5) shows the cross-correlation functions at $S/N = 10$ with different noise distributions. We conclude that for a given S/N ratio, the distribution of noise does not have a significant influence on the final cross-correlation function.

4. Methodology and Numerical Procedures

4.1. Cosmological Simulations and Simulated Spectra

In this work, we used data from 6 simulations with different values of Ω_Λ as discussed in §2.2. Before more QSO pairs are available from Sloan Digital Sky Survey (SDSS), approximately a few dozen QSO pairs with good quality should be observed through Keck (Kirkman et al. 2002). To provide an useful statistical study, we have to generate several groups of simulated pairs where each group has approximately the same number of pairs as are available observationally. We also know that pairs with angular separations between $1' - 3'$ contains good information of geometry in their cross-correlation functions (McDonald

et al. 1999). Therefore, we generated 300 paired QSO spectra with an angular separation of 120" using the spectrum generator code described in §3.1. Then we degraded the ideal QSO spectra to a FWHM of 300 km/s and a pixel size of 130 km/s, which is comparable to the LRIS of the Keck telescope. Gaussian-distributed noise with S/N = 10 and 20 were also added to the degraded simulated LRIS spectra. These values were chosen comparable with observational data which will be available in the near future.

4.2. Cross-Correlation Functions

Given a pair of QSO spectra, we first calculated the overflux at each point of a spectrum. The overflux δ_f and the mean flux \bar{f} are defined in § 3.2. However instead of considering one QSO spectrum as we did in § 3.2, we now have a pair of QSO spectra, so the mean flux \bar{f} is averaged over the whole data points of the paired spectra. Therefore we have :

$$\begin{aligned} & \delta_{f1}(z_1), \delta_{f1}(z_2), \dots \delta_{f1}(z_n) \text{ from the first QSO spectrum} \\ & \delta_{f2}(z_1), \delta_{f2}(z_2), \dots \delta_{f2}(z_n) \text{ from the second QSO spectrum} \end{aligned}$$

where z_i , $i = 1, 2, \dots n$, are the corresponding redshifts at each point of the QSO spectra. Thus for a point $\delta_{f1}(z_i)$ from the first spectrum and another point $\delta_{f2}(z_j)$ from the second spectrum, their parallel velocity separation can be expressed as:

$$\Delta v_{\parallel} \equiv c \frac{|z_j - z_i|}{1 + \bar{z}} \quad (11)$$

where $|z_j - z_i|$ are small and $\bar{z} = \frac{z_1 + z_n}{2}$. The cross-correlation at a given parallel velocity separation Δv_{\parallel} is denoted by $\xi(\Delta v_{\parallel})$ and is calculated by :

$$\xi(\Delta v_{\parallel}) = \langle \delta_{f1}(z_i) \delta_{f2}(z_j) \rangle \quad (12)$$

averaging over all possible permutations of (i,j) which satisfy Equation (11).

Figure (6) shows the cross-correlation functions of two QSO pairs (the first and second pair from the 300 pairs in the $\Omega_{\Lambda} = 0.7$ simulation). The significant difference of the cross-correlation function of the two pairs reveals the significant impact of cosmic variance, which is why we introduced the MLE method (see Appendix (A) and §4.4 for more detail).

4.3. Probability Distribution Functions

In order to apply the maximum likelihood method (MLE) to our analysis work, we need to provide accurate probability distribution functions first (Appendix (A)). For each of the 6 simulations, we have generated 300 paired QSO spectra with an angular separation of $120''$, providing 300 cross-correlation functions per simulation: $\xi(\Delta v_{\parallel} ; \Delta \theta | \Omega_{\Lambda})$, where $\Delta \theta = 120''$ and $\Omega_{\Lambda} = 0.0, 0.5, 0.6, 0.7, 0.8$ and 0.9 . We denote $\xi(\Delta v_{\parallel} ; \Delta \theta | \Omega_{\Lambda})$ for given $\Delta \theta$ and Ω_{Λ} at a fixed Δv_{\parallel}^* as $\xi(\Delta v_{\parallel}^*)$. At a given Δv_{\parallel}^* each cross-correlation function provides one value of $\xi(\Delta v_{\parallel}^*)$, so we have 300 data points of $\xi(\Delta v_{\parallel}^*)$ at Δv_{\parallel}^* under given Ω_{Λ} and $\Delta \theta$. The values of $\xi(\Delta v_{\parallel}^*)$ range between -0.02 and 0.03 . Using 50 bins spaced evenly between -0.02 and 0.03 , which are the upper and lower limits of the cross-correlation values, we bin the 300 data points of $\xi(\Delta v_{\parallel}^*)$. This gives us a probability distribution function of $\xi(\Delta v_{\parallel}^*)$ at Δv_{\parallel}^* , denoted by $\text{PDF}(\xi(\Delta v_{\parallel}^*))$, for known Ω_{Λ} and $\Delta \theta$. We repeat the procedures for different Δv_{\parallel} and Ω_{Λ} . Figures (7), (8) and (9) show the $\text{PDF}(\xi(\Delta v_{\parallel}^*))$ at three different Δv_{\parallel}^* for different cosmological models.

4.4. The Likelihood Calculation

Given a QSO pair, pair A, we first calculate the corresponding cross-correlation function $\xi_A(\Delta v_{\parallel})$ based on Equation (12). As mentioned in §1, the cross-correlation below and around 600 km/s contains information on cosmological parameters Ω_{Λ} and we denote these points as $(\Delta v_{\parallel}^1, \xi_A(\Delta v_{\parallel}^1)), (\Delta v_{\parallel}^2, \xi_A(\Delta v_{\parallel}^2)), \dots, (\Delta v_{\parallel}^m, \xi_A(\Delta v_{\parallel}^m))$. In our work, we use five points: $(\Delta v_{\parallel}^1 = 129.49 \text{ km/s}, \xi_A(\Delta v_{\parallel}^1))$, $(\Delta v_{\parallel}^2 = 258.99 \text{ km/s}, \xi_A(\Delta v_{\parallel}^2))$, $(\Delta v_{\parallel}^3 = 388.48 \text{ km/s}, \xi_A(\Delta v_{\parallel}^3))$, $(\Delta v_{\parallel}^4 = 517.97 \text{ km/s}, \xi_A(\Delta v_{\parallel}^4))$ and $(\Delta v_{\parallel}^5 = 647.47 \text{ km/s}, \xi_A(\Delta v_{\parallel}^5))$. For each given Ω_{Λ} , using the $\text{PDF}(\Delta v_{\parallel}^i | \Omega_{\Lambda})$ generated in §4.3, we then find that the probability of getting $(\Delta v_{\parallel}^i, \xi_A(\Delta v_{\parallel}^i))$ is f_A^i , where $i = 1, 2, 3, \dots, 5$. Therefore, the desired likelihood of the cross-correlation from pair A is $L_A = \prod_{i=1}^5 f_A^i$. By repeating the above procedures in different cosmological simulations, we can derive a likelihood function $L(\Omega_{\Lambda})$. By maximizing the likelihood function, we can determine Ω_{Λ} . Figure (10) shows the likelihood of two randomly chosen pairs with $S/N = 10$ and $S/N = 20$ (these are the same pairs shown in Figure (6)). Notice that we cannot determine Ω_{Λ} using only the information shown in the graph, which implies data from one pair of QSO spectra does not contain enough information for us to obtain Ω_{Λ} . Therefore, a combined-likelihood calculation from many pairs is necessary in order to obtain a useful result.

If we have more than one paired QSO spectra: $P_{A1}, P_{A2}, \dots, P_{Ar}$ with corresponding likelihoods: $L_{P_{A1}}, L_{P_{A2}}, \dots, L_{P_{Ar}}$, Then the combined-likelihood of all pairs is (see Appendix (A)):

$$L_{combined} = L_{P_{A1}} L_{P_{A2}} \dots L_{P_{Ar}} \quad (13)$$

The value in Equation (13) gives us the combined-likelihood value in one cosmology. The advantage of using the MLE method here is that we can derive Ω_Λ without collecting many paired QSO spectra with the same angular separation and redshift to determine a reliable cross-correlation function first.

5. Results

5.1. Probability of Obtaining the Correct value of Ω_Λ

To investigate the question about the number of pairs needed for deriving a reliable value of Ω_Λ , we take 300 paired QSO spectra from our $\Omega_\Lambda = 0.7$ simulation and pretend that they are observational data from the real Universe. First, we resample our 300 paired QSO spectra into 30 subgroups of 10 pairs each. As described in §4.4, in each subgroup we calculated the likelihood based on the data points of the 10 cross-correlation functions and then derived the combined-likelihood of the total 10 pairs in different cosmological models. Thus, in each subgroup, we derive a likelihood function of Ω_Λ . By maximizing the likelihood function (or the *log(likelihood)* function (LLK)), we derive the corresponding Ω_Λ (see Appendix (A) for details). Thus we have a distribution for values of Ω_Λ based on the 30 subgroups as shown in Figure (11). If we parametrize the distribution as a Gaussian, we find that Ω_Λ is 0.6 ± 0.145 .

Here we have assumed that the real value of Ω_Λ in the Universe is 0.7 and thus the 20 % error of Ω_Λ ranges from 0.56 to 0.84. Therefore, by calculating

$$P = \int_{0.56}^{0.84} dx \frac{1}{\sqrt{2\pi}\sigma} \exp\left[-\frac{1}{2} \frac{(x - \mu)^2}{\sigma^2}\right] \quad (14)$$

where $\mu = 0.6$ and $\sigma = 0.145$, we find that the probability of getting Ω_Λ within 20 % error is 56 %. Similarly, the 10 % error for the value of Ω_Λ ranges from 0.63 to 0.77. So by replacing the lower and the upper integration limits in Equation (14) to 0.63 and 0.77, we derived the probability of obtaining Ω_Λ with 10 % error is 30 %. By repeating the above procedures, we also conclude that the probability of getting Ω_Λ within 5 % error ($0.665 \leq \Omega_\Lambda \leq 0.735$) is 15 %.

Instead of sampling our 300 paired QSO spectra to 30 subgroups with 10 pairs in each subgroup, we also resampled the 300 paired-spectra into 20 subgroups with 15 pairs in each

subgroup, 15 subgroups with 20 pairs in each subgroup, 12 subgroups with 25 pairs in each subgroup and 10 subgroups with 30 pairs in each subgroup. Then in each case we calculated the distribution of Ω_Λ and the probability of deriving Ω_Λ within 20%, 10% and 5% errors. For the case we have 30 paired QSO spectra in each subgroup (10 subgroups), the probability of obtaining correct Ω_Λ within 20 % error is 94.15%, within 10 % error is 66% and within 5 % error is 36%. A complete result is displayed in Table (1). Each row in the table indicates one statistical study. The first column is the number of QSO pairs in one subgroup while the second column is the number of subgroups in each study. The third column denotes the result of Ω_Λ . Finally, the fourth, fifth, and the sixth columns are the probability of getting Ω_Λ within 20%, 10% and 5% error.

5.2. Error Propagation From Noise to Ω_Λ

Based on the method described in Appendix (B), we can propagate the noise from flux spectra to the final combined-likelihood function. We denote the upper limit of the error in estimations of Ω_Λ due to noise as $\sigma_{+,SN}$ and the lower limit as $\sigma_{-,SN}$. Then, with the same sets of simulations, we first took the 300 paired spectra with $S/N = 10$ and divided them into 10 subgroups (30 pairs per subgroup). As shown in Figure (12), in each subgroup the value of Ω_Λ is the point corresponding to the maximum LLK value. Then the value $LLK_{max} - \frac{1}{2}E_{noise}$ corresponds to two other values of Ω_Λ : $\Omega_\Lambda + \sigma_{+,SN}$ and $\Omega_\Lambda + \sigma_{-,SN}$, where E_{noise} is the error in LLK due to noise. By averaging the results of 10 subgroups, we found that the mean value of Ω_Λ equals 0.67 with $\sigma_{-,S/N=10} = 0.382$ and $\sigma_{+,S/N=10} = 0.244$. Comparing this result with the error from cosmic variance calculated in §5.1, the error due to noise is much larger than that due to cosmic variance. Therefore, spectra with higher S/N are desired. So we increased the signal-to-noise ratio to $S/N = 20$ and repeated the analysis describing previously. Similarly, with 30 pairs, we have the mean value of Ω_Λ equals 0.67 with $\sigma_{-,S/N=20} = 0.142$ and $\sigma_{+,S/N=20} = 0.113$. (see Figure (12)). In this case, the error in Ω_Λ due to noise is comparable to that due to cosmic variance. Therefore, we conclude that $S/N = 20$ is the minimum acceptable noise level if only 30 QSO pairs are available.

6. Discussion and Conclusion

Even though the possibility of using the AP test on the Ly α forest to measure Ω_Λ has been emphasized (Hui et al. 1999; McDonald et al. 1999), the practical work of dealing with real observational data is not easy. There are several major difficulties in this work including cosmic variance, uncertainty of other cosmological parameters, understanding of spectral

resolution along with S/N properties and the continuum fitting. This paper focuses on producing noisy low resolution spectra which are comparable with the real LRIS observational data and how to defeat the errors due to noise and cosmic variance.

Based on the study of noisy low resolution spectra generated from our simulation as discussed in §3.2, we have found that degrading resolution decreases the amplitude of the flux power spectrum. This is because the convolution procedure smoothes out structures in the original flux spectra. On the other hand, adding artificial noise into the QSO spectra increases the amplitude of the flux power spectrum, especially for $k \geq 0.1$ rad/(km/s). This is because random noise and small structures in the flux spectra are indistinguishable. Therefore, we conclude that data in k-space beyond $k = 0.1$ rad/(km/s) is untrustworthy for our purposes.

In order to handle the cosmic variance problem, we introduced the MLE technique in the analysis procedures. We then conclude that based on 30 paired QSO spectra with an angular separation of $120''$, we have 94% confidence to determine Ω_Λ within 20 % error, 66% confidence to determine Ω_Λ within 10 % error and 36 % confidence to determine Ω_Λ within 5 % error. Here we have taken the spectral resolution into account and the cosmic variance is overcome. From Table (1) and §5.2, we conclude that the error due to cosmic variance is already smaller than the errors due to the noise based on 30 QSO pairs. Therefore it is more important to obtain high S/N quality spectra. The spectra with $S/N \geq 20$ are desirable in order to derive a reliable value of Ω_Λ (§5.2).

The process of gathering paired QSO spectra is time-consuming. Even before enough QSO pairs have been gathered to constrain the value of Ω_Λ , we can achieve a useful result by ruling out unlikely models. Under the assumption that we live in a universe with a high value for Ω_Λ , we can rule out the SCDM model at 90 % confidence by utilizing only 10 pairs of QSO spectra if we assume the the other cosmological parameters are known (Figure (11)). This will be the next step in our project. Some other important topics of this work including taking care of the error propagation due to continuum fitting and the uncertainty of other cosmological parameters. More detailed work of these issues are under investigation and will be discussed in the near future.

We highly appreciate Brian O’Shea, Tridevish Jena and Pascal Paschos for helping editing and organizing the article. We also grateful to the useful discussions with Tridevish Jena and Professor Tytler’s group including Nao Suzuki, David Kirkman and John O’Meara. This work is supported by NSF grant AST-9803137 under the auspices of the Grand Challenge Cosmology Consortium.

REFERENCES

- Abel, T. et al. 1997, *New Astronomy*, 2, 181
- Alcock, C. & Paczynski, B. 1979, *Nature* 281, 358
- Anninos, P. et al. 1997, *New Astronomy*, 2, 209
- Bahcall, N. 2000, *Physical Scripta*, T85, 32-36
- Bahcall, N. & Fan, X. 1998, *ApJ*, 504, 1
- Bardeen, J. M. et al. 1986, *ApJ*, 304, 15
- Ballinger, W. E., Peacock, J.A., & Heavens, A.F. 1996, *MNRAS* 292, 877
- Burles, S., Nollett, K., Truan, J. and Turner, M. S. 1999, *Phys. Rev. Lett.* 82, 4176
- Carlstrom, J., et al. 2000, *Physical Scripta*, T85, 148-155
- Copi, C. J., Schramm, D. N. & Turner, M. S. 1995, *Science*, 267, 192.
- Frigo, M. & Johnson, S.G. 1998, *ICASSP*, 3, pp. 1381-1384
- Frodesen et al. 1978, *Probability and Statistics in Particle Physics*
- Goobar, A. et al. 2000, *Physical Scripta*, T85, 47-58
- Guerra, E. J., Daly, R. A. and Wan, L. 2000, *ApJ*, 544, 659-670
- Haardt, F. & Madau, P. 1996, *ApJ*, 461, 20
- Harrison, D. M. 2001, *Error Analysis in Experimental Physical Science*
- Hata, N. et al. 1995, *Phys. Rev. Lett.*, 75, 3977
- Holder, G. et al. 2001, *ApJ*, 560, L111-L114
- Hui, L. et al. 1999, *ApJ*, 511, L5
- Kirkman et al. 2002, private communication
- Matsubara, T. & Suto, Y. 1996, *ApJ*, L1
- McDonald, P. et al. 1999. *ApJ*, 528, 24
- Meiksin, A. & Madau, P. 1993, *ApJ*, 412, 34

- Melchiorri, A. et al. 2000, ApJ, 536, L63-L66
- Mohr, J., Mathiesen, B. and Evrard, A. E. 1998, ApJ, 517, 627
- Peacock, J. & Dodds, S. 1994, MNRAS, 267, 1020.
- Peebles, P.J.E. 1984, ApJ, 284, 439.
- Perlmutter, S. et al. 1999, ApJ, 517, 565
- Popowski, P. A., Weinberg, D. H., Ryden, B.S., & Osmer, P.S. 1998, ApJ, 498, 11
- Press, W.H., Teukolsky, S.A., Vetterling, W.T., Flannery, B.P. 1998, Numerical Recipes
- Rauch, M. et al. 1997, ApJ, 489, 7.
- Riess, A. et al. 1998, ApJ, 116, 1009
- Ryden, B.S. 1995, ApJ, 452, 25
- Turner, M. S. 1983, Phys. Rev. D, 28, 1243.
- Tytler, D., Fan, X.-M., Burles, S., Cottrell, L. Davis, C., Kirkman, D., & Zuo, L. 1995, in QSO Absorption Lines, ed. G. Meylan (Berlin: Springer), 289
- Weinberg, D. et al. 1997, ApJ, 490, 546
- White, S.D.M. et al. 1993, Nature 366, 429
- Zhang, Y. et al. 1997, ApJ, 485, 496
- Zhang, Y. et al. 1998, ApJ, 495, 63

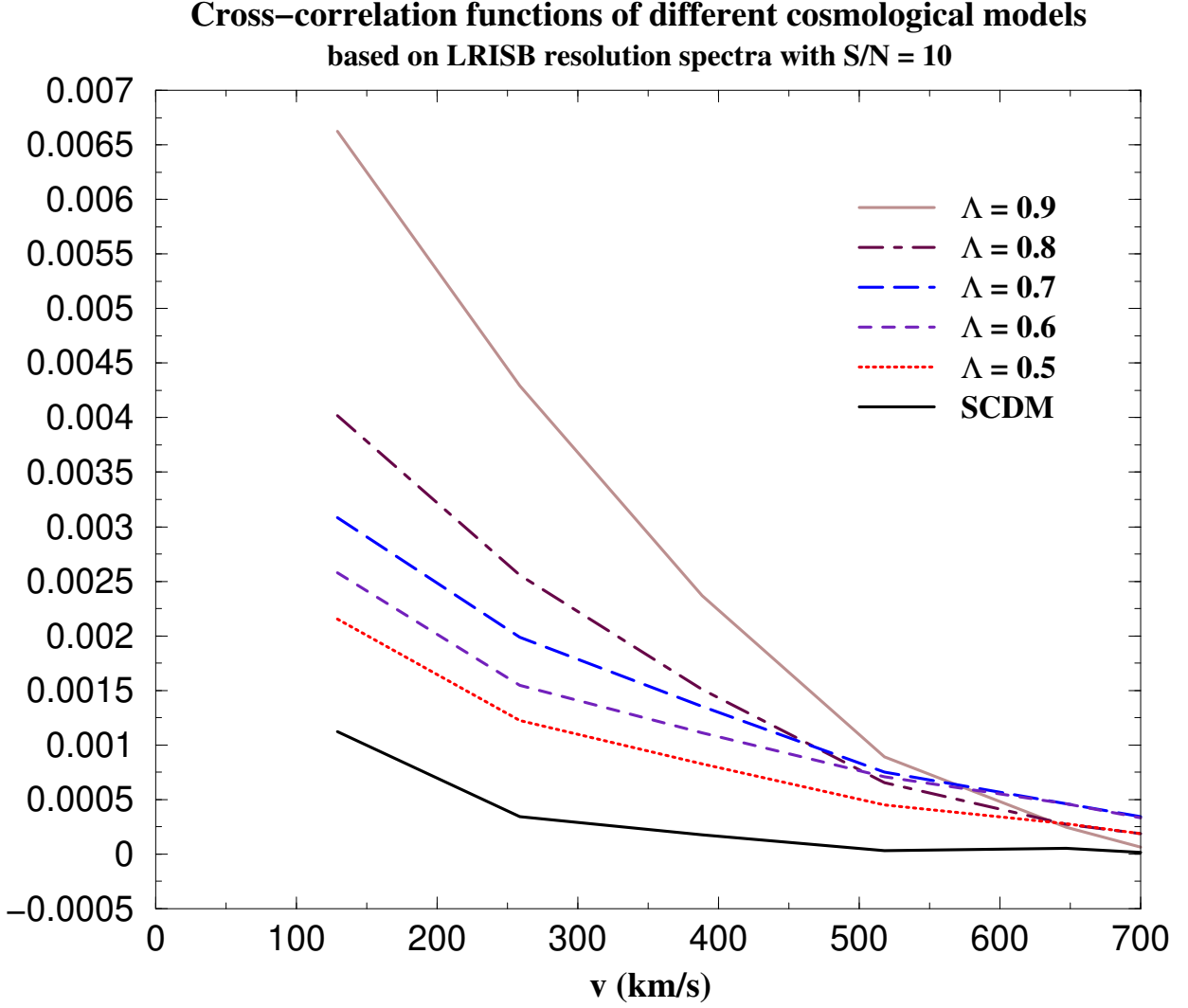


Fig. 1.— Flux cross-correlation functions for several cosmological models with different Ω_Λ . Each curve is the average of 300 cross-correlation functions while each cross-correlation function was derived from a paired QSO spectra based on our simulations. The corresponding FWHM is 300 km/s, the pixel size is 130 km/s and the signal-to-noise ratio is 10. The angular separation is 120". The lower solid curve is the SCDM model and the higher solid curve is the $\Omega_\Lambda = 0.9$ model. The dotted curve is the $\Omega_\Lambda = 0.5$ model, the dashed curve is the $\Omega_\Lambda = 0.6$ model, the long-dashed curve is the $\Omega_\Lambda = 0.7$ model and the dotted-dashed curve is the $\Omega_\Lambda = 0.8$ model.

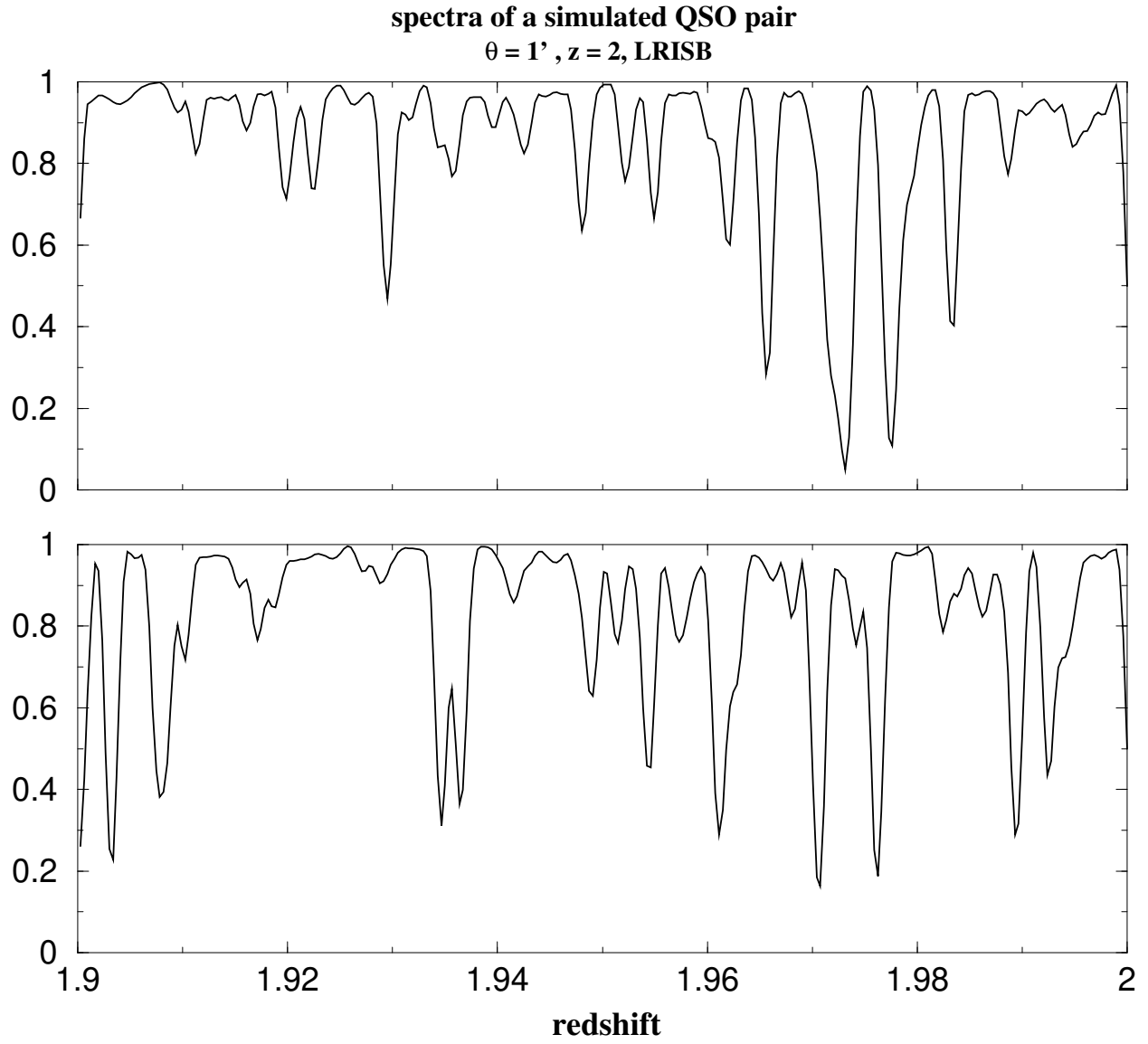


Fig. 2.— A pair of simulated QSO spectra at $z=2$. The spectra were degraded to LRIS resolution with a FWHM of 300 km/s and a pixel size of 130 km/s. The angular separation of the QSO pair is $1'$.

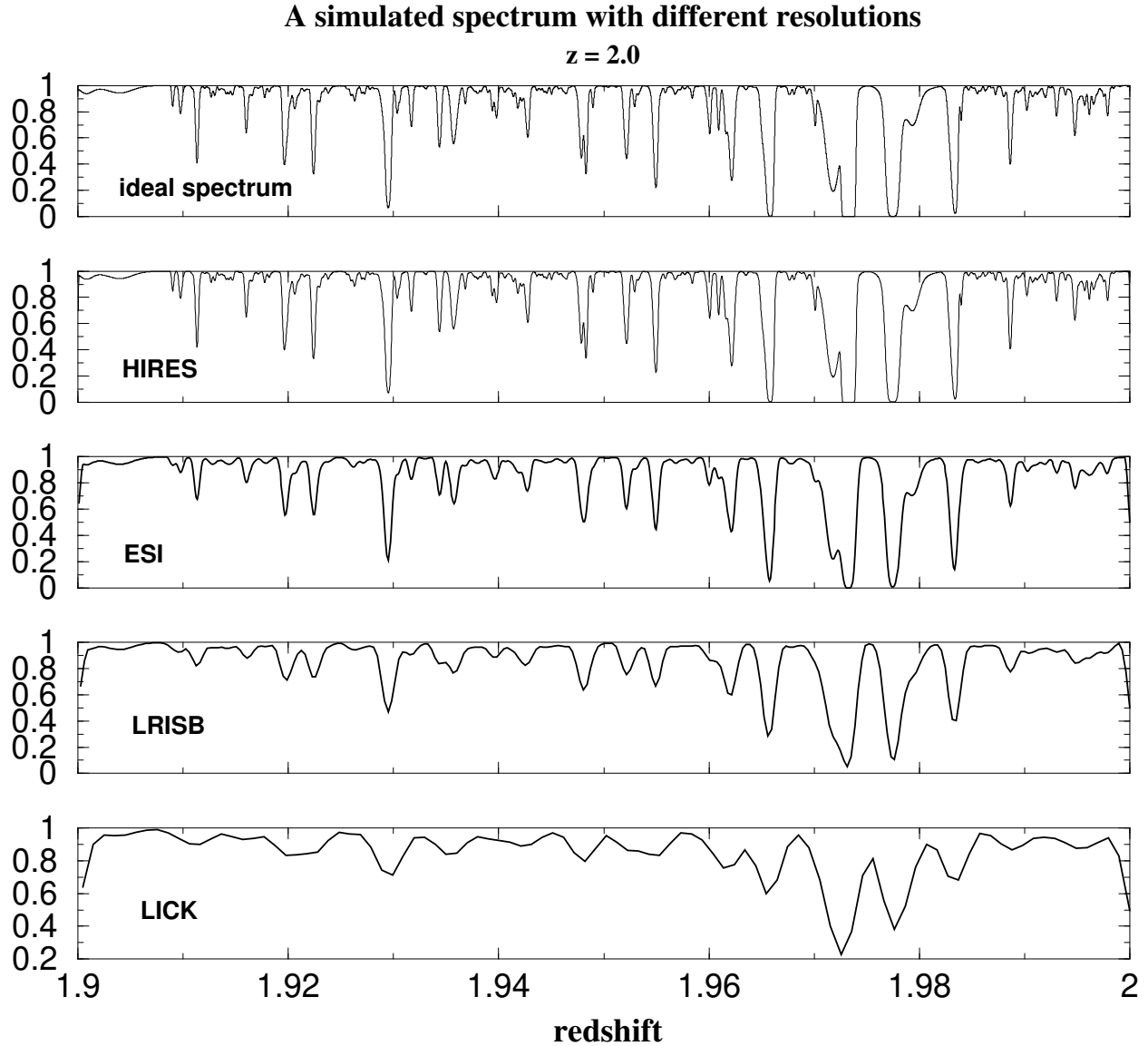


Fig. 3.— We degraded an ideal flux spectrum from our simulation to different resolutions based on desired instruments. HIRES: High Resolution Echelle Spectrometer of the Keck telescope, FWHM = 8 km/s. ESI: An Echellette Spectrograph and Imager for the Keck II Telescope, FWHM = 55 km/s. LRIS: Low Resolution Imaging Spectrometer resolution of the Keck telescope, FWHM = 115 - 300 km/s (115 km/s in this Figure). Lick: FWHM: 250 km/s.

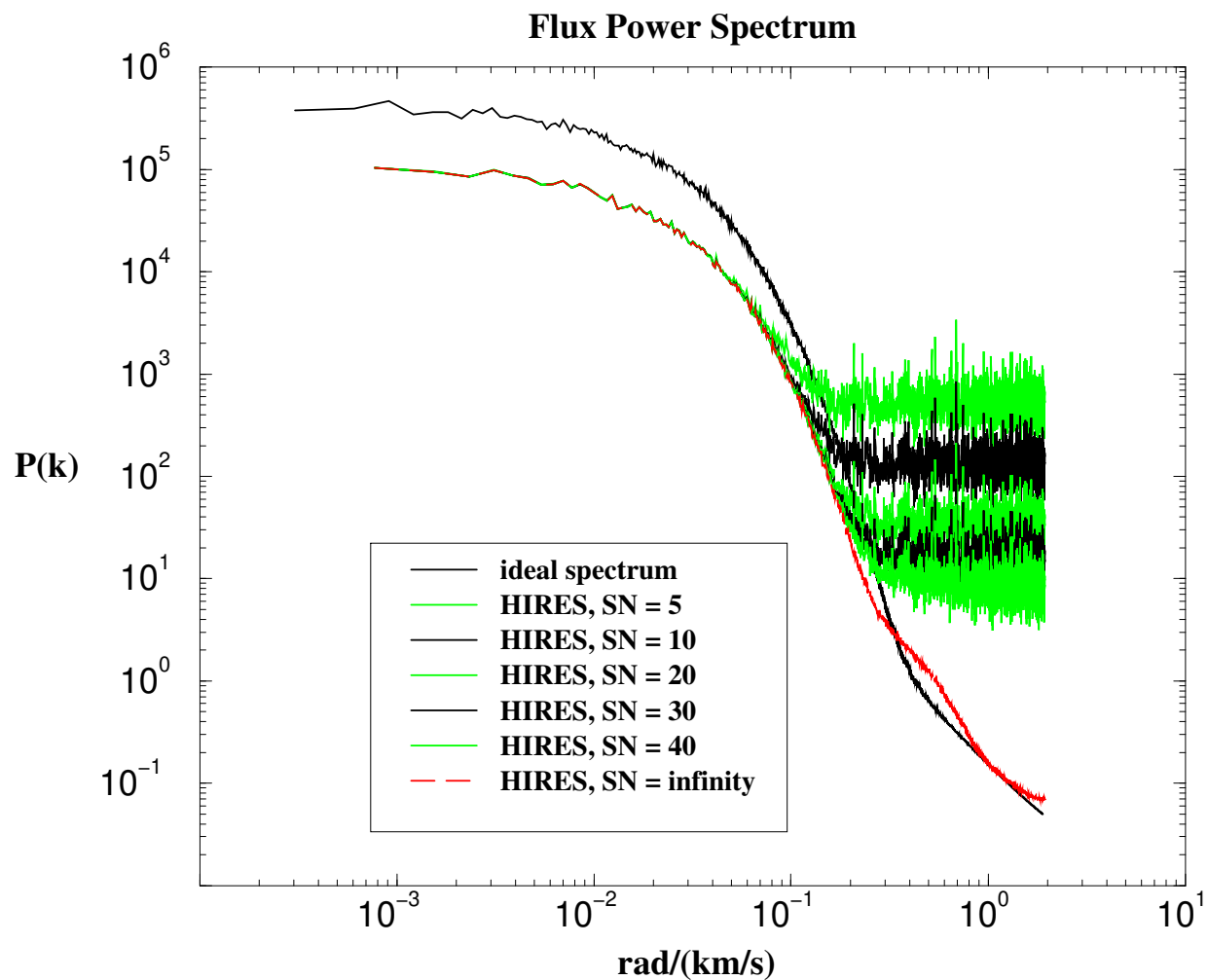


Fig. 4.— The averaged flux power spectrum based on 300 simulated QSO spectra. We degraded the ideal spectra to HIRES resolution and then added different amounts of noise. The highest solid curve is from the ideal spectra and the lowest long dashed curve is with the HRIES resolution without any noise. There are five noisy curves in the middle, which are with $\text{SN} = 40$, $\text{SN} = 30$, $\text{SN} = 20$, $\text{SN} = 10$ and $\text{SN} = 5$ from low to high, respectively.

**Cross-correlation functions of different noise distribution
based on LRIS resolution spectra with $S/N = 10$**

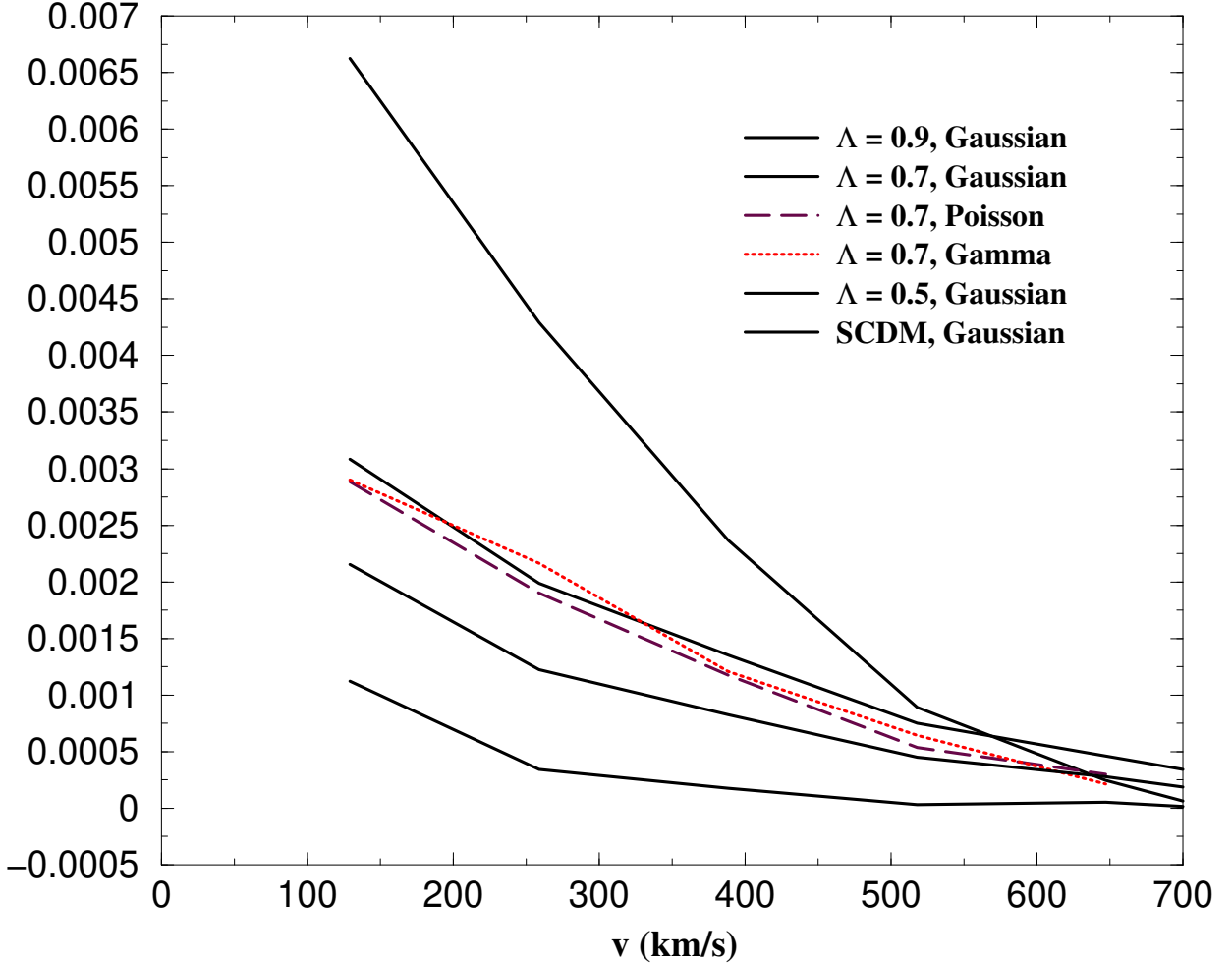


Fig. 5.— Flux cross-correlation functions with different noise distribution. Each curve is the average of 300 cross-correlation functions while each cross-correlation function was derived from a paired QSO spectra based on our simulations. The corresponding FWHM is 300 km/s, the pixel size is 130 km/s and the signal-to-noise ratio is 10. The angular separation is 120". The four solid curves are SCDM (the lowest solid curve), $\Omega_\Lambda = 0.5$ (the second lowest solid curve), $\Omega_\Lambda = 0.7$ (the second highest solid curve) and $\Omega_\Lambda = 0.9$ (highest solid curve) cosmological models with Gaussian noise. The long dashed curve is the $\Omega_\Lambda = 0.7$ cosmological model with Poisson noise distribution and the dotted curve is the $\Omega_\Lambda = 0.7$ cosmological model with Gamma noise distribution.

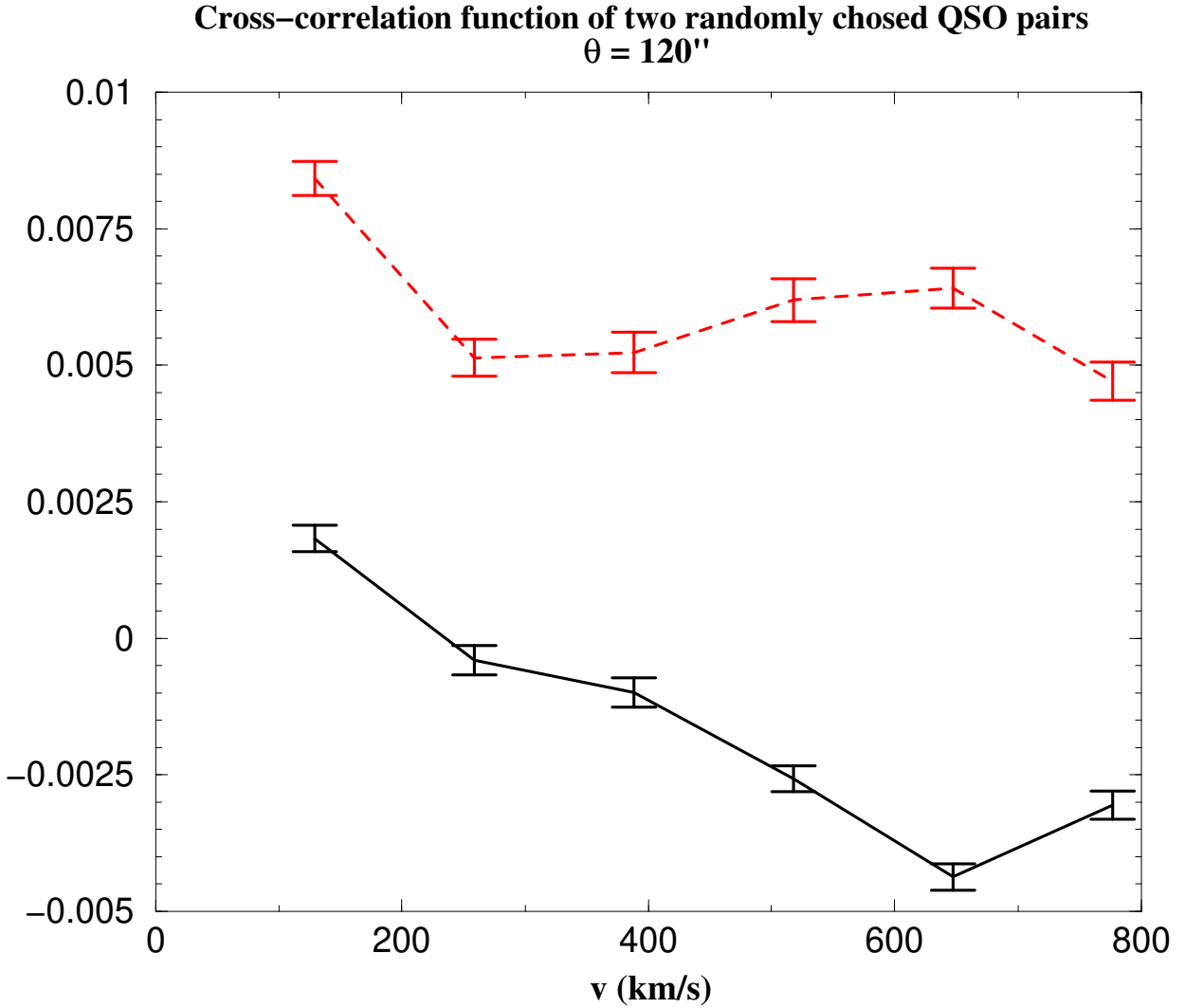


Fig. 6.— Flux cross-correlation functions for the first and the second QSO pair of the 300 pairs from the $\Omega_\Lambda = 0.7$ simulation. The solid line denotes the result of the first pair while the dashed line denotes the result of the second pair. The error bars were propagated from the flux spectra with $S/N = 10$. The angular separation is $120''$.

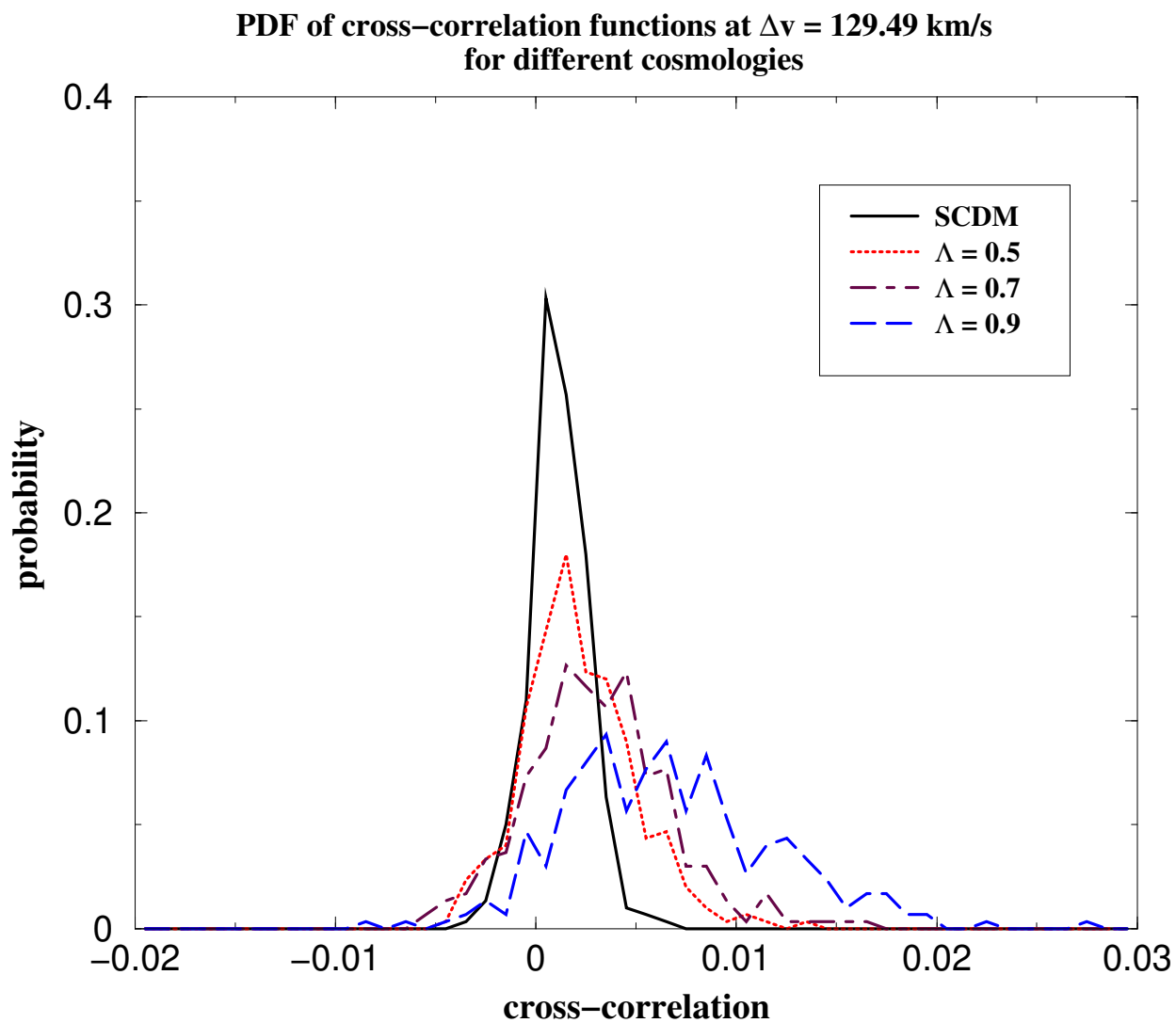


Fig. 7.— PDF($\xi(\Delta v_{\parallel}^*)$) of cosmological models with different Ω_{Λ} . The x-axis is the flux cross-correlation and the y-axis is the probability. The Δv_{\parallel}^* equals to 129.49 km/s. The pair separation is $120''$. The solid curve is the SCDM model, the dotted curve is the $\Omega_{\Lambda} = 0.5$ model, the dotted-dashed curve is the $\Omega_{\Lambda} = 0.7$ model and long-dashed curve is the $\Omega_{\Lambda} = 0.9$ model.

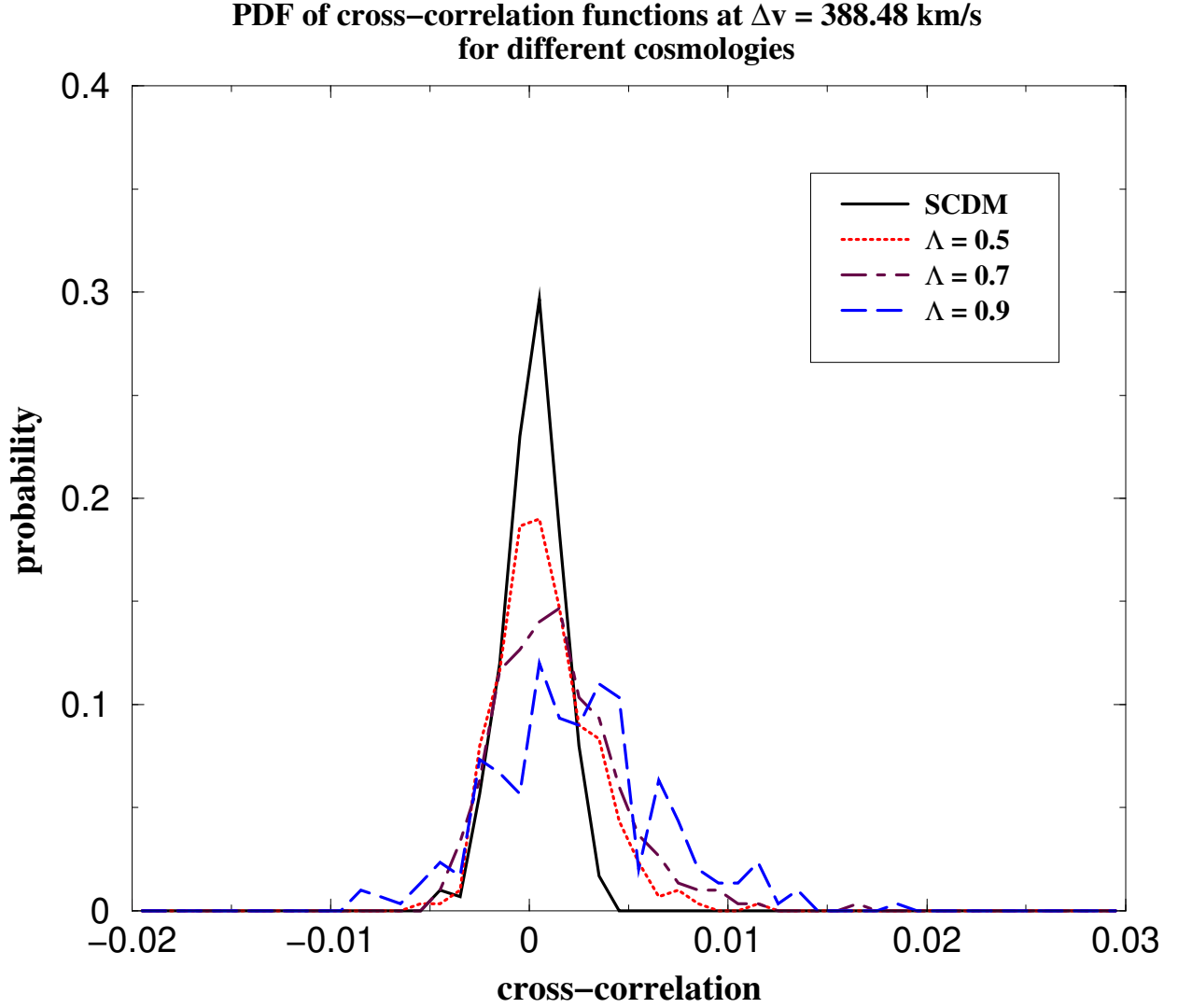


Fig. 8.— PDF($\xi(\Delta v_{\parallel}^*)$) of cosmological models with different Ω_{Λ} . The x-axis is the flux cross-correlation and the y-axis is the probability. The Δv_{\parallel}^* equals to 388.48 km/s. The pair separation is $120''$. The solid curve is the SCDM model, the dotted curve is the $\Omega_{\Lambda} = 0.5$ model, the dotted-dashed curve is the $\Omega_{\Lambda} = 0.7$ model and long-dashed curve is the $\Omega_{\Lambda} = 0.9$ model.

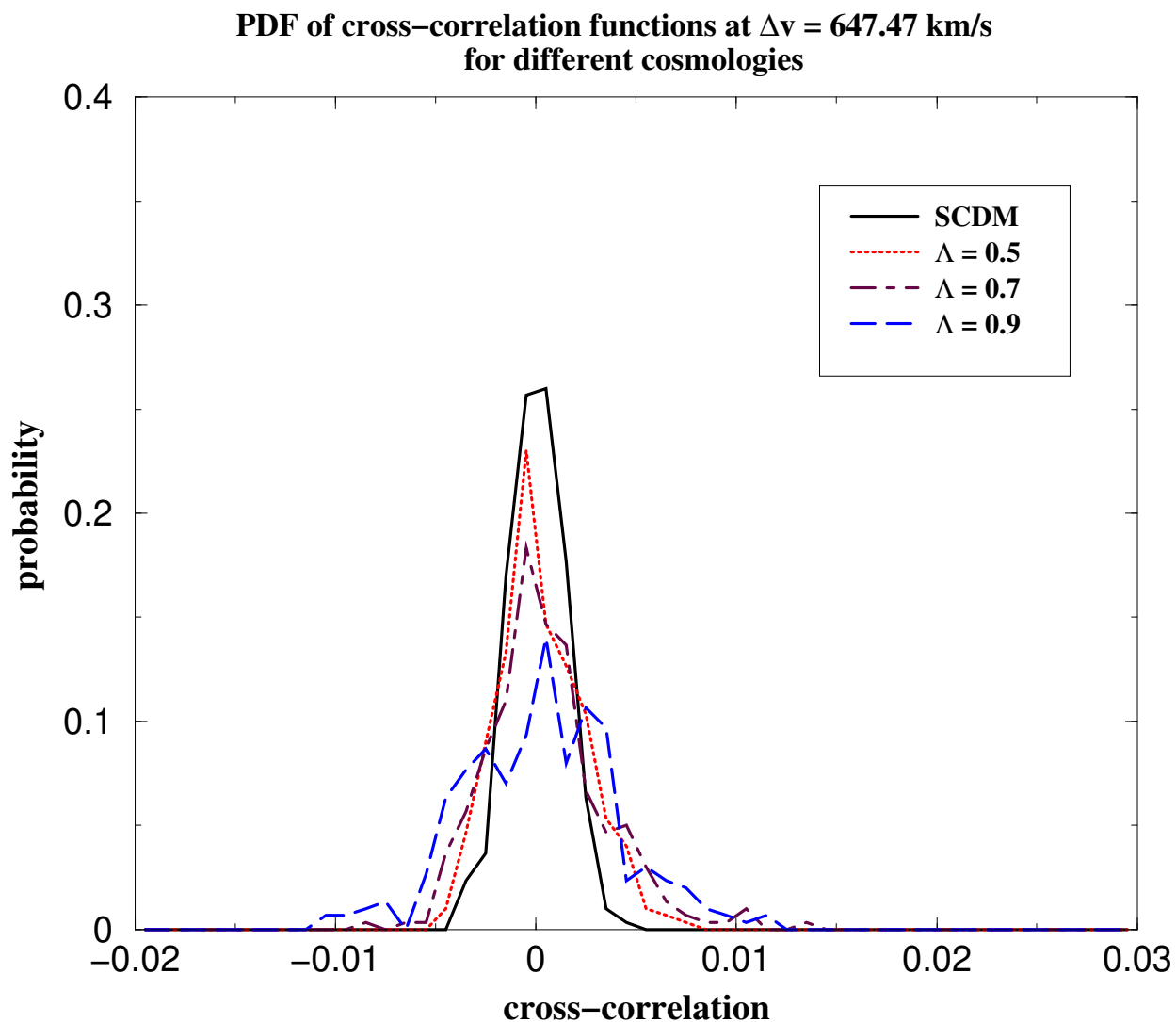


Fig. 9.— PDF($\xi(\Delta v_{\parallel}^*)$) of cosmological models with different Ω_{Λ} . The x-axis is the flux cross-correlation and the y-axis is the probability. The Δv_{\parallel}^* equals to 647.47 km/s. The pair separation is $120''$. The solid curve is the SCDM model, the dotted curve is the $\Omega_{\Lambda} = 0.5$ model, the dotted-dashed curve is the $\Omega_{\Lambda} = 0.7$ model and long-dashed curve is the $\Omega_{\Lambda} = 0.9$ model.

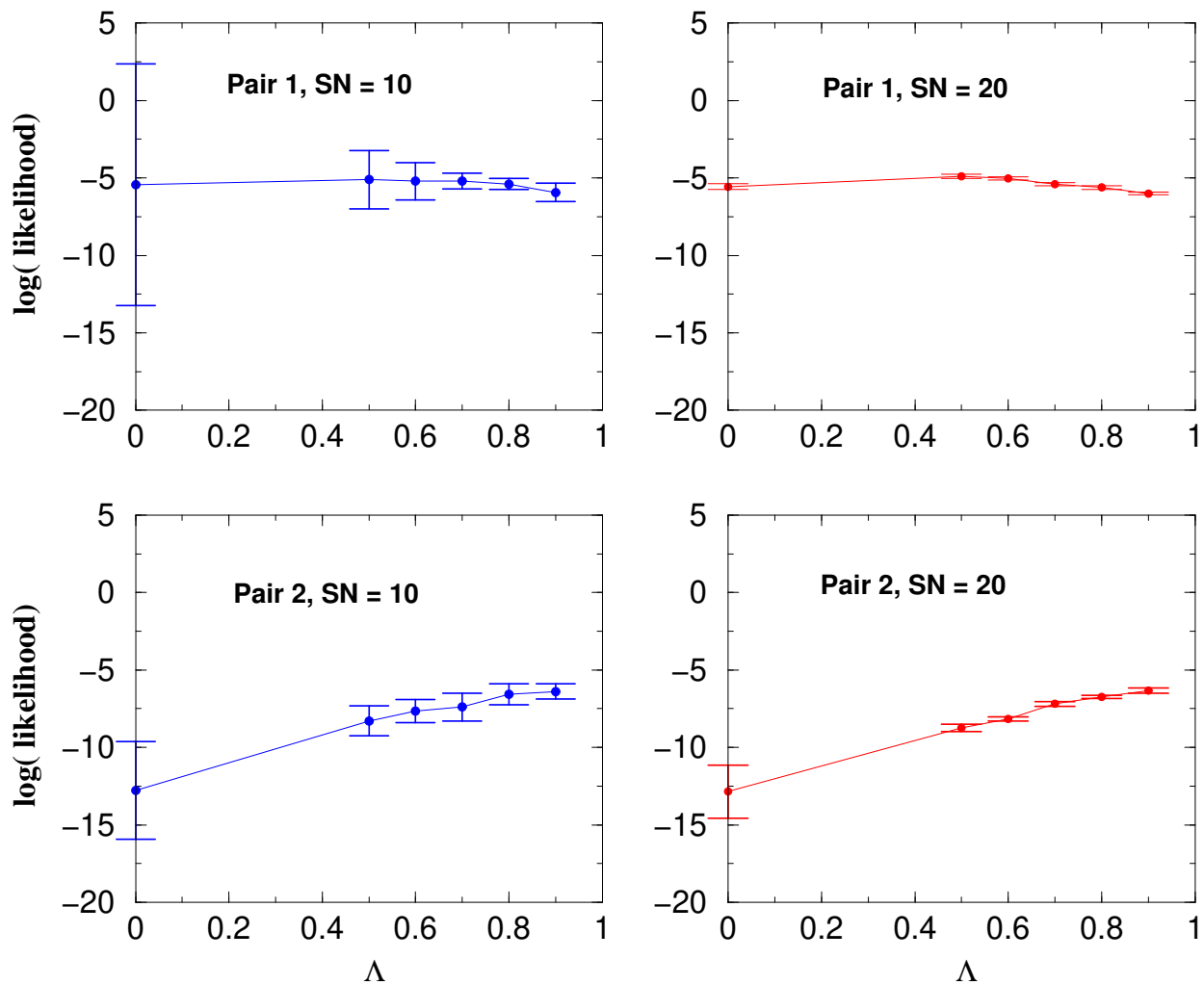


Fig. 10.— $\log(\text{likelihood})$ functions of two randomly chosen QSO pairs with $S/N = 10$ and $S/N = 20$. (The first and the second pair of the 300 pairs from the $\Omega_\Lambda = 0.7$ simulation.) The pair separation is $120''$. We should pay more attention to the lower half of the error which statistically contains more physical meanings (see Appendix (C)).

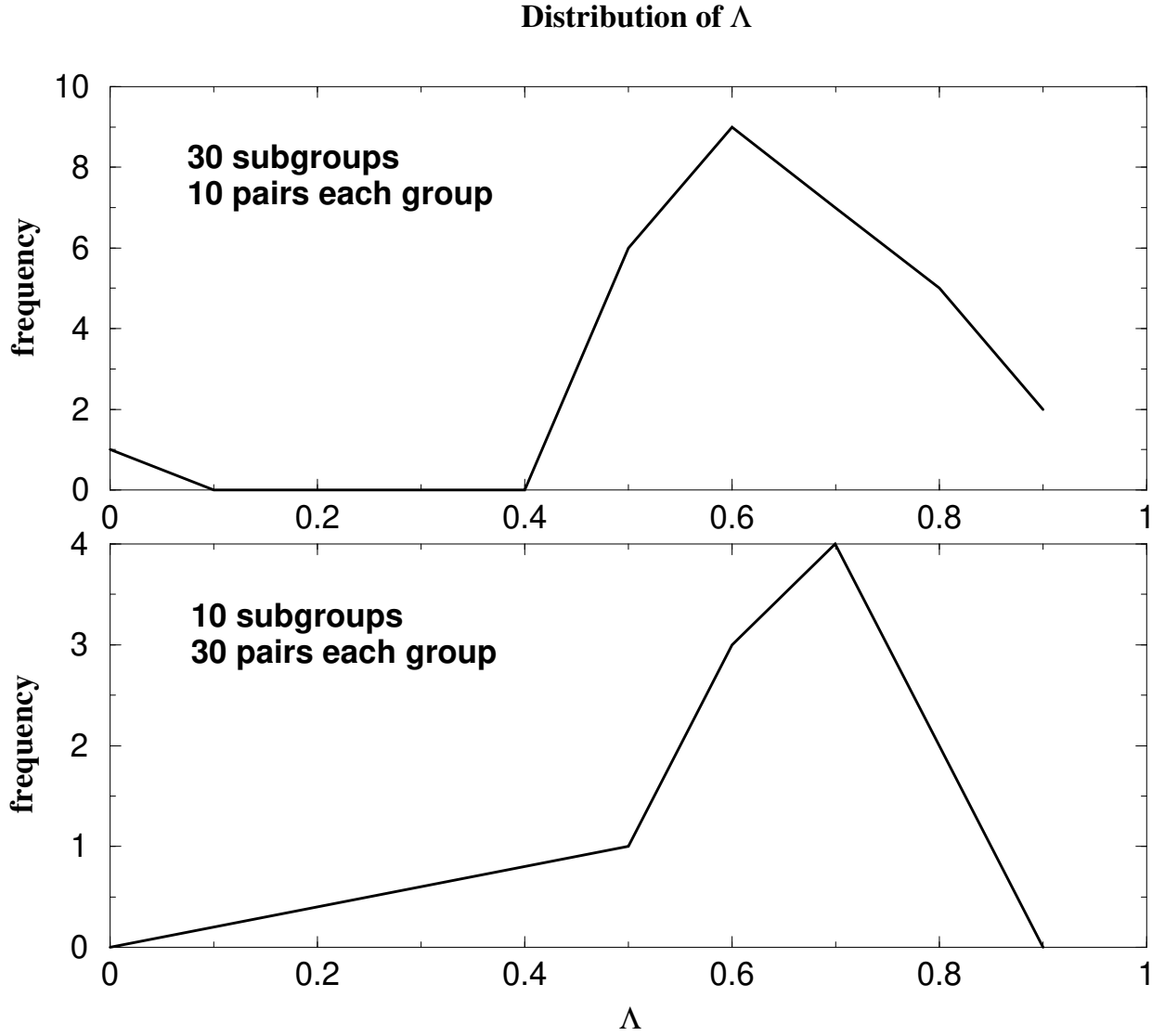


Fig. 11.— The distributions of Ω_Λ based on 10 paired QSO spectra (30 subgroups) and 30 paired QSO spectra (10 subgroups). We have assumed Ω_Λ in the Universe is 0.7.

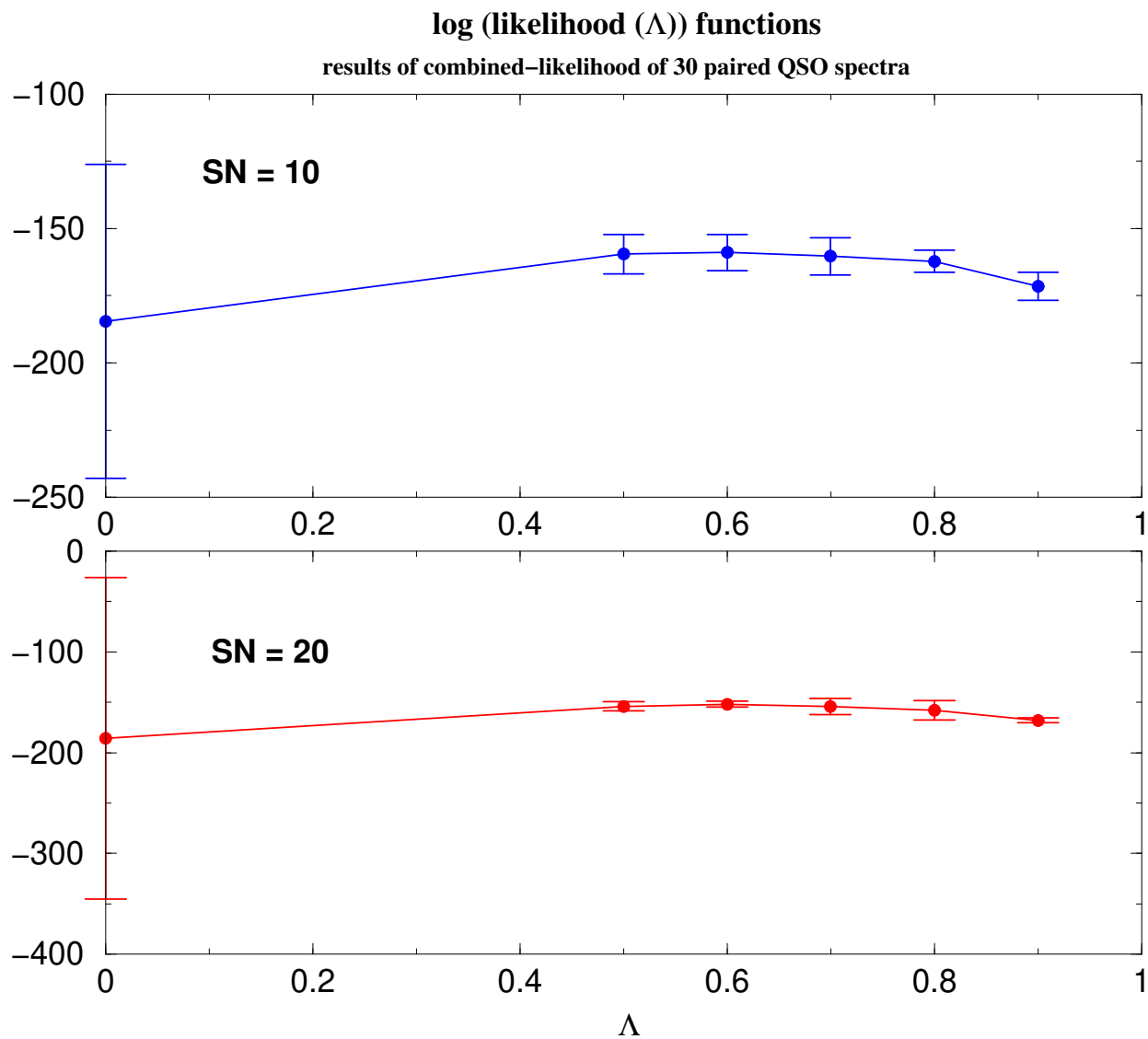


Fig. 12.— $\log(\text{likelihood})$ functions based on 30 paired QSO spectra with $S/N = 10$ and $S/N = 20$. The x-axis denotes the value of Ω_Λ and the y-axis denotes the value of $\log(\text{likelihood})$. We have assumed Ω_Λ in the Universe is 0.7. We should pay more attention to the lower half of the error which statistically contains more physical meanings (see Appendix (C)).

$\frac{\text{pairs}}{\text{group}}$	gp #	Ω_Λ	P(20%)	P(10%)	P(5%)
10	30	0.6 ± 0.15	56 %	30 %	15 %
15	20	0.6 ± 0.1	64 %	34 %	17 %
20	15	0.64 ± 0.1	77 %	44 %	23 %
25	12	0.7 ± 0.1	80 %	48 %	25 %
30	10	0.7 ± 0.07	94 %	66 %	36 %

Table 1: Probability of getting Λ within 20%, 10% and 5% error. Each row in the table indicates on statistical study. The first column is the number of QSO pairs in one subgroup while the second column is the number of subgroups in each study. The third column denotes the result of Ω_Λ . Finally, the fourth, fifth, and the sixth columns are the probability of getting Ω_Λ within 20%, 10% and 5% error.

A

A. Maximum-Likelihood Estimation

For a random sample x_1, x_2, \dots, x_n from a population with a probability distribution function (PDF) depending on a parameter θ , the function $t = t(x_1, x_2, \dots, x_n)$ is called a "statistic" if it does not depend on any other unknown parameters. Then the term "estimator" denotes a function, method or prescription used to find a value of an unknown parameter. In general, t is an estimator of the unknown θ . For a continuous or discrete population which has probability distribution $f(x | \theta)$, the likelihood of n observations x_1, x_2, \dots, x_n for a specific θ is given by

$$L(x_1, x_2, \dots, x_n | \theta) = \prod_{i=1}^n f(x_i | \theta) \tag{A1}$$

We can think of $L(x_1, x_2, \dots, x_n | \theta)$ as a function of θ and call it the "likelihood function", denoted by L or $L(\underline{x} | \theta)$. To be more general, if we consider n independent experiments with the same physical parameter θ from these n sets, $\underline{x}_1, \underline{x}_2, \dots, \underline{x}_n$, of observations, the corresponding likelihood functions of each set are $L(\underline{x}_1 | \theta)$, $L(\underline{x}_2 | \theta)$, ..., and $L(\underline{x}_n | \theta)$, respectively. Then the combined-likelihood of all observations is :

$$L(\underline{x}_1, \underline{x}_2, \dots, \underline{x}_n | \theta) \equiv \prod_{i1} f_1(x_{i1} | \theta) \prod_{i2} f_2(x_{i2} | \theta) \dots \prod_{in} f_n(x_{in} | \theta) \tag{A2}$$

which is equivalent to

$$\log(L(\underline{x}_1, \underline{x}_2, \dots, \underline{x}_n | \theta)) \equiv \log(f_1(x_{i1} | \theta)) + \sum_{i2} \log(f_2(x_{i2} | \theta)) + \dots + \sum_{in} \log(f_n(x_{in} | \theta)) \tag{A3}$$

Maximizing the combined likelihood in Equationd (A2) or its equivalent expression in Equation (A3) gives us an estimation of θ denoted by $\hat{\theta}$ (Frodesen et al. 1978). In this work, the unknown parameter θ is chosen to be Ω_Λ . Each x_i is a data point in the corresponding cross-correlation function. The probability distribution function $f_i(x_i | \theta)$ is the PDF of the cross-correlation at a velocity separation for a given Ω_Λ while other parameters are fixed (Details are described in §4.3 and §4.4).

B

B. Error Propagation

One important issue in this work is how errors in the flux spectra propagate to the likelihood functions. Let $E[f(x_0)]$ denote the error of any given function $f(x)$ at x_0 . As mention in §4.2, the mean flux \bar{f} of a paired QSO spectra:

$$\bar{f} = \frac{\sum_{i=1}^n (f_1(z_i) + f_2(z_i))}{2n} \quad (\text{B1})$$

where n is the number of points in a spectrum, $f_1(z_i)$ and $f_2(z_i)$, $i=1, 2, \dots, n$ are the data points from the first and second flux spectra of a QSO pair. Then based on the error propagation formulas (Harrison, 2001) we have

$$E[\bar{f}] = \frac{\sqrt{\sum_{i=1}^n E[f_1(z_i)]^2 + E[f_2(z_i)]^2}}{2n} \quad (\text{B2})$$

where $E[f_1(z_i)]$ is the error of the point $f_1(z_i)$ and $E[f_2(z_i)]$ is the error of the point $f_2(z_i)$. For the overflux $\delta f = \frac{f - \bar{f}}{\bar{f}}$, we have $E[f - \bar{f}] = \sqrt{E[f]^2 + E[\bar{f}]^2}$. So

$$E(\delta f) = E\left[\frac{f - \bar{f}}{\bar{f}}\right] = \delta f \sqrt{\frac{E[f - \bar{f}]^2}{(f - \bar{f})^2} + \left(\frac{E[\bar{f}]}{\bar{f}}\right)^2} = \delta f \sqrt{\frac{E[f]^2 + E[\bar{f}]^2}{(f - \bar{f})^2} + \left(\frac{E[\bar{f}]}{\bar{f}}\right)^2} \quad (\text{B3})$$

When the noise is random and the number of data points are large, $E[\bar{f}]$ is negligible. In this case, we can assume :

$$E[\delta f(z_i)] \sim \frac{1}{(S/N)} \delta f(z_i) \quad (\text{B4})$$

From §4.2, $\xi(\Delta v_{\parallel}) = \langle \delta_{f_1}(z_i) \delta_{f_2}(z_j) \rangle$, where the average is over all possible (i,j) permutations. We consequently get

$$E[\delta_{f_1}(z_i) \delta_{f_2}(z_j)] = \delta_{f_1}(z_i) \delta_{f_2}(z_j) \sqrt{\left(\frac{E[\delta_{f_1}(z_i)]}{\delta_{f_1}(z_i)}\right)^2 + \left(\frac{E[\delta_{f_2}(z_j)]}{\delta_{f_2}(z_j)}\right)^2} \quad (\text{B5})$$

Therefore,

$$E[\xi(\Delta v_{\parallel})] = \frac{1}{N} \sqrt{\sum_{i,j} \left(\frac{E[\delta_{f_1}(z_i) \delta_{f_2}(z_j)]}{\delta_{f_1}(z_i) \delta_{f_2}(z_j)}\right)^2} \quad (\text{B6})$$

where N is the number of all possible (i,j) permutations. Thus, if the probability of having $\xi_A(\Delta v_{\parallel}^*)$ at Δv_{\parallel}^* is $f_A(\xi_A(\Delta v_{\parallel}^*))$, we can also get the upper and lower probability limits:

$$f_{A,upper} = f_A(\xi(\Delta v_{\parallel}^*) + \frac{1}{2}E[\xi(\Delta v_{\parallel}^*)]) \quad (B7)$$

$$f_{A,lower} = f_A(\xi(\Delta v_{\parallel}^*) - \frac{1}{2}E[\xi(\Delta v_{\parallel}^*)]) \quad (B8)$$

then the error range of the final probability is:

$$E[f_A(\xi(\Delta v_{\parallel}^*))] = f_{A,upper} - f_{A,lower} \equiv E[f_A^*] \quad (B9)$$

Then next step is to propagate the errors to the likelihood functions. As mentioned in §4.4, the likelihood of pair A is $L_A = \prod_{i=1}^m f_A^i$ ($m=5$ in this paper). Therefore,

$$\log(L_A) = \sum_{i=1}^m (\log f_A^i) = F(f_A^1, f_A^2, \dots, f_A^m) \quad (B10)$$

$$\begin{aligned} E[\log L_A]^2 &= \left(\frac{\partial \log L_A}{\partial f_A^1}\right)^2 E[f_A^1]^2 + \left(\frac{\partial \log L_A}{\partial f_A^2}\right)^2 E[f_A^2]^2 + \dots + \left(\frac{\partial \log L_A}{\partial f_A^m}\right)^2 E[f_A^m]^2 \\ &= \left(\frac{1}{L_A} \frac{\partial L_A}{\partial f_A^1}\right)^2 E[f_A^1]^2 + \left(\frac{1}{L_A} \frac{\partial L_A}{\partial f_A^2}\right)^2 E[f_A^2]^2 + \dots + \left(\frac{1}{L_A} \frac{\partial L_A}{\partial f_A^m}\right)^2 E[f_A^m]^2 \\ &= \left(\frac{E[f_A^1]}{f_A^1}\right)^2 + \left(\frac{E[f_A^2]}{f_A^2}\right)^2 + \dots + \left(\frac{E[f_A^m]}{f_A^m}\right)^2 \end{aligned} \quad (B11)$$

This is because $L_A = \prod_{i=1}^m f_A^i$ and $\frac{\partial L_A}{\partial f_A^i} = \prod_{j=1, j \neq i}^m f_A^j$.

So

$$E[\log L_A] = \sqrt{\sum_{i=1}^m \left(\frac{E[f_A^i]}{f_A^i}\right)^2} \quad (B12)$$

Therefore, the error of \log [combined-likelihood of m pairs] are:

$$E[\log L_{combined}] = \sqrt{\sum_{i=1}^m E[\log L_{P_{Ai}}]^2} \quad (B13)$$

C

C. Errors in the Probability

We should pay more attention to the lower half of the error bars in the final likelihood function. To see this, consider n probability functions and their corresponding probability ranges :

$$f_1 - \Delta f_1 \leq f_1 \leq f_1 + \Delta f_1$$

$$f_2 - \Delta f_2 \leq f_2 \leq f_2 + \Delta f_2$$

...

$$f_n - \Delta f_n \leq f_n \leq f_n + \Delta f_n$$

Therefore, the final mean probability $f_{mean} = f_1 f_2 \dots f_n$, and the upper and lower limits of the probabilities are :

$$\text{upper limit : } f_{upper} = (f_1 + \Delta f_1)(f_2 + \Delta f_2) \dots (f_n + \Delta f_n)$$

$$\text{lower limit : } f_{lower} = (f_1 - \Delta f_1)(f_2 - \Delta f_2) \dots (f_n - \Delta f_n)$$

Here we argue that with large amount of data points, the final combined probability $f_{combined}$ should fall between f_{lower} and f_{mean} . To simplify the problem, let $f_1 = f_2 = \dots = f_n = f$, and $\Delta f_1 = \Delta f_2 = \dots = \Delta f_n$. Then

$$f_{upper} = (f + \Delta f)^n$$

$$f_{lower} = (f - \Delta f)^n$$

On the average, consider $n=2m$ data points, we can assume m data points with probability $\geq f$ and are equal to $(f + \frac{1}{2}\Delta f)$. Similarly, there are m data points with probability $\leq f$ and are equal to $(f - \frac{1}{2}\Delta f)$. Therefore the final combined probability should be :

$$f_{combined} = (f - \frac{1}{2}\Delta f)^m (f + \frac{1}{2}\Delta f)^m = (f^2 - \frac{1}{4}\Delta f^2)^m \leq f^{2m} = f^n = f_{mean}$$

$$\Rightarrow f_{lower} \leq f_{combined} \leq f_{mean}$$

So with large amount of data points, the lower half of the error bars contains more physical meanings.